ACS APPLIED NANO MATERIALS

www.acsanm.org Article

# Silver Nanoparticle-Decorated Personal Protective Equipment for Inhibiting Human Coronavirus Infectivity

Mutalifu Abulikemu, Bita E. A. Tabrizi, Shahrokh M. Ghobadloo, Hamed M. Mofarah, and Ghassan E. Jabbour*

Cite This: *ACS Appl. Nano Mater.* 2022, 5, 309−317 Read Online

ACCESS | Metrics & More | Article Recommendations | Supporting Information

**ABSTRACT:** The Coronavirus disease 2019 (COVID-19) global outbreak and its continued growth and mutation into various forms emphasize the need for effective disinfectants to assist in the reduction of the virus's spread from individual to individuals and community to communities through various modes, including coughing, sneezing, touching of contaminated surfaces, and being in proximity of an unprotected infected person, to mention a few. The rapid development of reliable disinfecting materials or solutions and their incorporation in personal protective equipment is a critical need at the moment that will assist significantly in curbing the spread of the virus SARS-CoV-2, the cause of COVID-19 illness. Here, we present an *in situ* assembly of antiviral metal nanoparticles on a rigid surface and on commercial face masks made up of nonwoven and woven textiles. The results indicate a very high efficacy of 99.99% against a surrogate virus to SARS-CoV-2. Such a versatile and cost-effective approach using the blade-coating technique can be easily extended to the roll-to-roll manufacturing setting to expedite the efforts and mitigate the rapid spread of the virus.

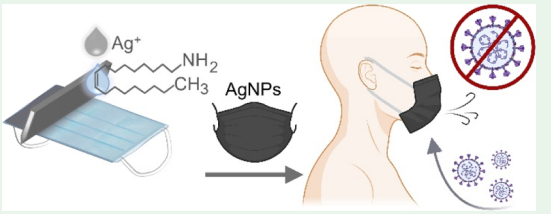


**KEYWORDS:** *silver nanoparticles, reactive coating, human coronavirus, COVID-19, SARS-CoV-2, roll-to-roll, face mask and textile*



## INTRODUCTION

The global outbreak of COVID-19 pandemic is causing an enormous health threat in the world, and it is affecting people at all levels, in particular, health workers who are most exposed to it. COVID-19 is caused by a new virus, SARS-CoV-2. SARS-CoV-2 is a genus family of coronaviruses (e.g., HCoV-229E, HCoV-NL63, and HCoV-OC43) infecting animals and humans and causing mild to critical illnesses such as the Middle East respiratory syndrome and acute respiratory syndrome (caused by SARS-CoV-1).[1−3] The major symptoms of SARS-CoV-2 infection of the upper respiratory tract in humans include cough, fever, and, in more severe cases, difficulty in breathing. The virus binds to human angiotensin-converting enzyme-2 (ACE2) receptors on the host cells and induces pneumonia and multisystem illness with the involvement of different organs and raises the potential for systemic complications.[2] A recent study has shown that SARS-CoV-2 virus can live for hours to days on surfaces such as countertops and doorknobs, and its lifetime (stability) depends on the material makeup of the surface.[4] Moreover, the virus easily transmits to individuals through respiratory droplet spread when a person talks, coughs, or sneezes. The best approach to prevent viral infections is vaccination; however, the development of vaccines accepted by the majority of the population is time-consuming and expensive and requires sophisticated equipment and lengthy protocols.[2,3,5−7] Alcohols, sodium hypochlorite, quaternary ammonium, hydrogen peroxide-containing products, and ultraviolet light are common and effective disinfectants for preventing virus transmission, but they require continuous application to the surface of interest for prolonged disinfection, which has unidentified side effects.[8,9] For instance, liquid disinfectants dry out from surfaces in a short time following application. Nanomaterials, due to their inherent antipathogenic ability, are necessary to consider as alternatives.[7,10−13] They have already been shown to play a noticeable role in developing efficient vaccines[14] or nanomedicine to block ACE2 binding and consequently inhibit viral replication.[2] Furthermore, the nanomaterial-based technology may provide unique self-disinfecting surface coatings that are long-lived, can inactivate viruses, and prevent human transmission while also improving the efficiency and safety of the air filter system and mask.[5,6,15,16]

Individual metals (e.g., Au, Ag, Cu, and Ce)[11,17−21] and metal oxide-based (e.g., $Cu_2O$, ZnO, and $CeO_2$)[20,22−26] nanoparticles (NPs) have been used as antibacterial and antiviral agents. Compared to other metal NPs, Ag NPs are widely employed for deactivating numerous viruses and bacteria due to their diversity, stability, low cost, and desirable efficacy. For example, silver (Ag) NPs have been used as

**Received:** September 20, 2021
**Accepted:** December 6, 2021
**Published:** December 21, 2021

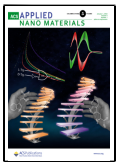

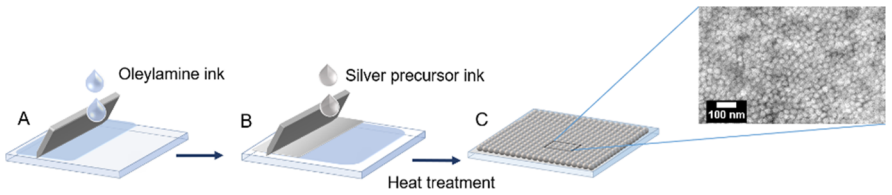


**Figure 1.** Schematic illustration of the reactive blade coating RC process of Ag NP-based thin film on glass. (A) A few droplets of the reducer ink with a 30 % V/V mixture of oleylamine in toluene (TOL) were deposited along one sidewall of the blade onto the glass substrate. (B) Precursor ink comprising 30 mg/mL silver nitrate $AgNO_3$ dissolved in dimethyl sulfoxide (DMSO) was blade coated on the top of the first reducing layer. (C) The blade-coated substrates, subsequently, were heated first at 80 °C for 1 h and then for 3 h at 120 °C resulting in the formation of Ag NPs.

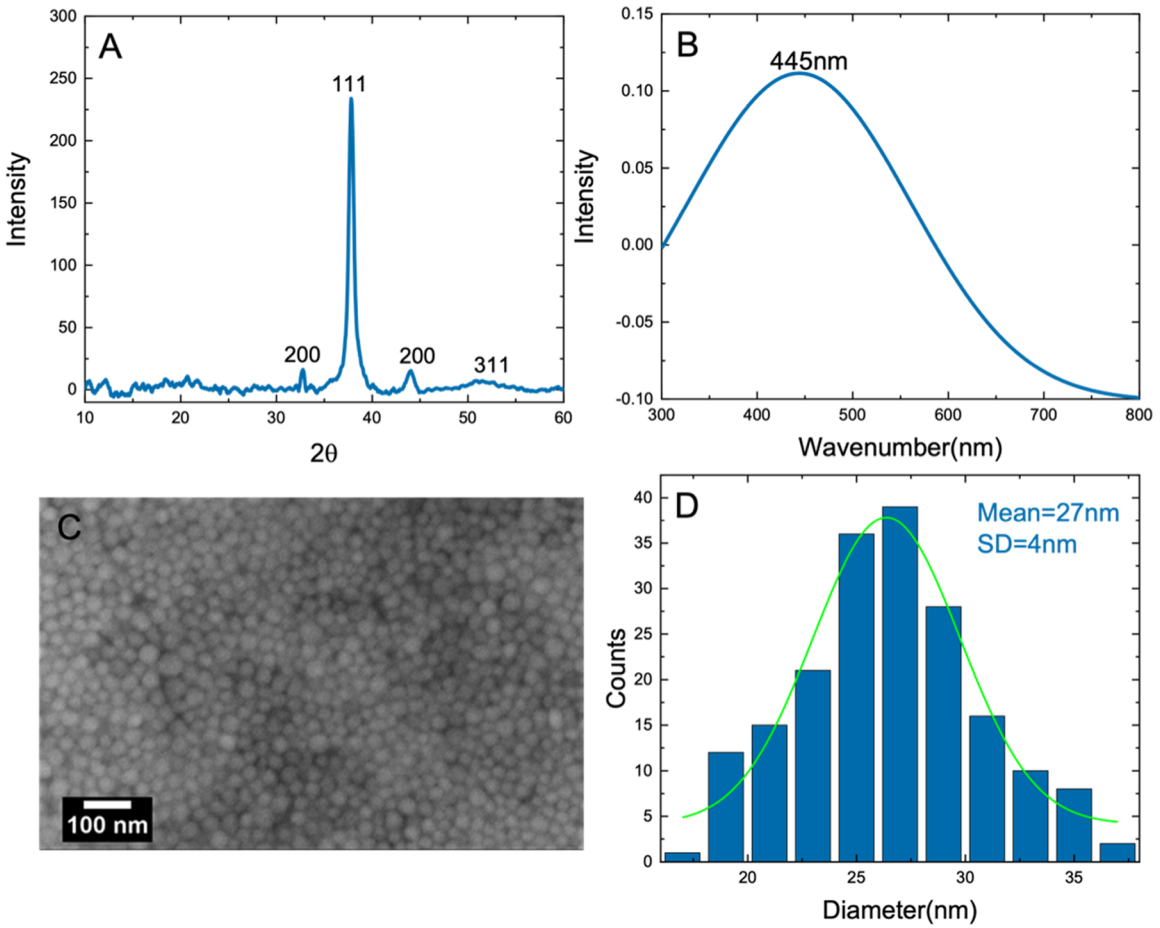


**Figure 2.** Characterization of the RC antiviral thin film. (A) X-ray diffraction spectrum showing an fcc structure of Ag NPs, (B) UV−vis spectrum indicating plasmonic absorption at ca. 445 nm, (C) SEM image showing the spherical shape of Ag NPs, and (D) histograms of synthesized Ag NPs. The mean size of Ag NPs is 27 nm with a standard deviation (SD) of 4 nm.

antibacterial (Gram-negative and Gram-positive bacteria), antifungal, antiviral, anti-inflammatory, and antiangiogenic agents. Several studies have recently revealed promising antiviral efficiency of Ag NPs against human immunodeficiency virus-1, hepatitis B virus, respiratory syncytial virus, herpes simplex virus type 1, monkeypox virus, influenza virus, and tacaribe virus.[17,27] Very recently, Balagna et al. sputtered a Ag nanocluster/silica composite (less than 200 nm in thickness) on a disposable facial FFP3 mask made of a nonwoven fabric. The coated mask showed a virucidal effect against coronavirus SARS-CoV-2.[28] During the preparation of our manuscript, two manuscripts reported the virucidal effect of a Ag NP solution and a Ag NP-impregnated polycotton fabric against SARS-CoV-2.[29,30] Besides, metal-oxide NPs, zinc oxide (ZnO)[22,24,25] and copper oxide (CuO)[23,26] NPs, have also shown antiviral and antibacterial effectiveness. On the other hand, researchers from the University of Arizona applied a proprietary antimicrobial surface coating made of a quaternary ammonium polymer on all hard and soft surfaces in selected medical units at a hospital and tested its efficacy against the human coronavirus 229E (HCoV-229E), which is similar in structure and genetics to SARS-CoV-2. Even 2 weeks after the coating was placed, it was capable of inactivating over 90 and 99.9% of the HCoV-229E within 10 min and 2 h, respectively.[31] Antimicrobial coatings, according to the same study, could provide an extra layer of protection, limiting the spread of coronaviruses in indoor spaces and public locations where contamination is constant.

Graphene oxide,[32] lignin molecules,[33] and NP-impregnated textiles/fabrics[29,34] have been studied for their antibacterial


https://doi.org/10.1021/acsanm.1c03033
ACS Appl. Nano Mater. 2022, 5, 309−317

and antiviral characteristics; however, most of these investigations have focused on *ex situ* coating of NPs on textiles utilizing pre-prepared liquids containing the NPs and/or physical deposition techniques.[29,32,33] It is also worth noting that graphene has been linked to cancer.[35] To our knowledge, no report of adopting a cost-effective *in situ*/reactive blade-coating (RC) technology to create NP coating on glass or impregnation into textiles for use as masks in the fight against SARS-CoV-2 has been published. In this paper, we demonstrate a low carbon footprint and cost-effective fabrication of antiviral coating on glass, textiles, and masks capable of achieving disinfection rates up to 99.99% when in contact with HCoV-229E, which is utilized as a surrogate for SARS-CoV-2 virus.

## RESULTS AND DISCUSSION

***In Situ* Synthesis of Ag NPs on Glass Substrates with Reactive Blade Coating.** A schematic representation of the *in situ* formation of the self-assembled Ag NPs using RC, a roll-to-roll (R2R) compatible deposition technique, is shown in Figure 1. The reducer ink (Figure 1A) was blade coated on a pre-cleaned glass slide (Premium Microscope Slides, Fisher Scientific), followed by coating silver precursor ink on top of the reducer ink (Figure 1B). The angle between the blade and the substrate was maintained at 50°, with respect to the substrate surface, during the coating process. After the coating steps, the substrate was heated first at 80 °C for 1 h followed by 120 °C for 3 h, yielding a colored thin coating over the substrate surface (Figure S1A).

Further investigation of the resulting coating using X-ray diffraction (XRD), Figure 2A, reveals a face-centered cubic (fcc) crystal structure of the as-synthesized Ag NPs, as expected for silver. The UV/vis absorption spectrum shows a strong plasmonic peak at approximately 445 nm (Figure 2B). Scanning electron microscopy (SEM) reveals the formation of densely packed self-assembled NPs. In this case, the average diameter of Ag NPs is approximately (27 ± 4) nm, as shown in Figure 2C. To determine the chemical composition of the NPs, energy-dispersive X-ray spectroscopy (EDS) was performed. The results (Figure S2) confirmed the presence of a pure phase of Ag on the substrate surface.

For reactive blade coating of Ag NPs, we also explored two additional solvent solutions. One uses TOL as a reducer and isopropanol (IPA) as a precursor solvent, while the other uses dichlorobenzene (DCB) as a reducer and *tert*-butyl alcohol (TBA) as a precursor solvent. Silver perchlorate hydrate ($AgClO_4{\cdot}xH_2O$) is employed as the silver precursor in both systems. After processing, the blade-coated films with the layers TOL/IPA and DCB/TBA were examined and compared to TOL/DMSO. In this regard, the SEM images and XRD spectrum are presented in Figure S3, which indicate that TOL/DMSO provides the best coverage and NP size homogeneity.

To assess the SARS-CoV-2 antiviral activity of a product, scientists commonly utilize HCoV-229E as a substitute for the SARS-CoV-2 virus.[25] This is mostly owing to the fact that access to a biosafety level 3 facility (which is required to handle the SARS-CoV-2 virus) is both expensive and limited. HCoV-229E, on the other hand, only requires a biosafety level 2 laboratory, which significantly lowers the cost of studies and is readily available at uOttawa. As noted earlier, both HCoV-229E and SARS-CoV-2 viruses belong to the family Coronaviridae, which comprise a group of enveloped, positive-sensed, single-stranded RNA viruses. The details of the virucidal efficacy test are described in the Materials and Method. The plaques developed by HCoV-229E in the L-132 cell monolayer are revealed in Figure 3A,B after 2- and 8 days

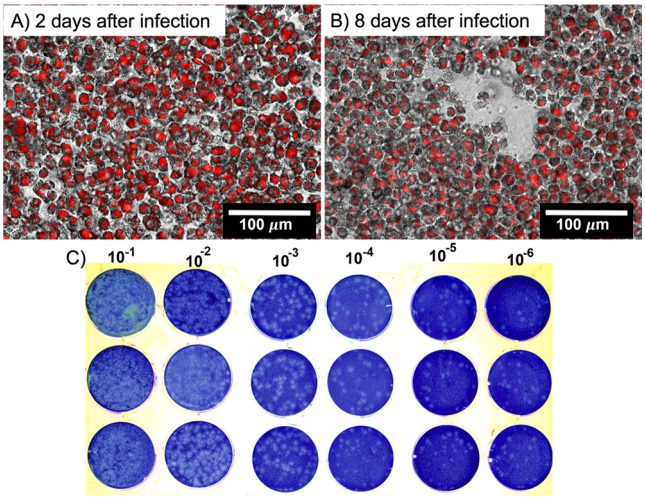


**Figure 3.** Progression of the plaque-forming assay. (A,B) Plaque development in L-132 cells in 2 days (A) and 8 days (B) after infection with HCoV-229E and overlaying with a mix of media, 2% L-glutamine and 10% fetal bovine serum (FBS), 0.5% low melting agarose, and 0.03% neutral red. Neutral red stains live cells by accumulating in live cells' lysosomes, and it was used to monitor plaque development. (C) Images of the HCoV-229E plaque-forming assay using L-132 cells. The monolayers of cultured L-132 cells were infected by 10 times serial dilution of the virus in the triplicate test format and overlayed with a mix of media, 2% FBS, and 0.5% low melting agarose after infecting the cells. The second layer was added 4 days after that. On day 8, the cells were fixed by 10% formaldehyde and stained by 0.5% crystal violet. The number of plaques in the constable wells were counted and multiplied with the test sample dilution factor of the related well, which is given by [HCoV-229E infectivity] plaque forming unit (PFU)/mL = (the combined numbers of plaques in the three wells with countable plaques/3) × (serial dilution factor) × (dilution factor from the sample).

of incubation. The L-132 cells were visualized with neutral red, which indicated that a significant number of cells were dead after 8 days of incubation time. The gray area in Figure 3B represents the formed plaques as a result of the infection and cells' death. Figure 3C depicts plaques formed by serial dilutions of HCoV-229E incubated with L-132 cells. More images of cell growth and confluence during plaque formation compared to control cells at different time points are shown in Figures S4 and S5. The infected cells were observed under a fluorescence microscope to determine the time when countable viral plaques appeared and have not yet diffused into one another's plaques. After the presentation of countable plaques, the cells were fixed with 10% formaldehyde and stained with 0.5% crystal violet to count plaques after incubation for 8 days.

To compare the virucidal effect of our RC-Ag NPs film with commercially available Ag NPs (labelled as C−Ag NPs), we coated C−Ag NPs ink (BotFactory, USA) on glass (Figure S1B) under the same conditions using the doctor-blade technique and tested its antiviral properties in parallel with our RC coatings. The RC-Ag NP-coated glass showed a strong virucidal effect against HCoV-229E (Figure 4). In this case, after 1 min, 91.89% of viruses were killed, and over 95% of them were eradicated after 10 min of incubation time. A more


https://doi.org/10.1021/acsanm.1c03033
ACS Appl. Nano Mater. 2022, 5, 309−317

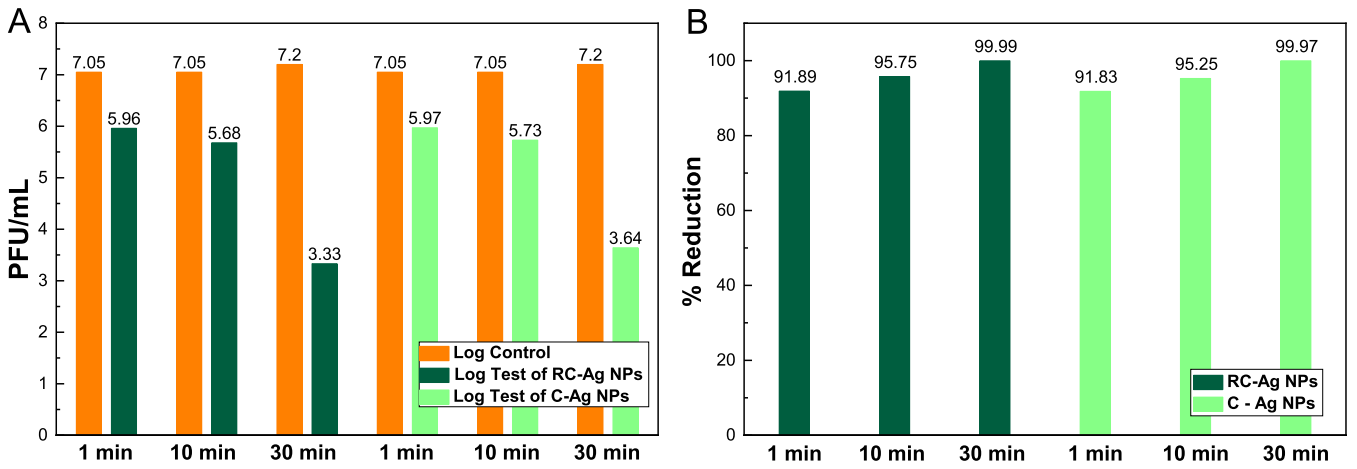


**Figure 4.** (A) Log geometric mean values of the HCoV-229E infectivity after contacting both thin films of RC-Ag NPs (dark green) and C−Ag NPs (bright green) for three different time intervals (1, 10, and 30 min) compared to those of controls having no contact with the thin films (orange). (B) The % reduction graph showing the values calculated from the infectivity test results, which are used to quantify the effectiveness of the NP-coated thin films to sanitize the HCoV-229E. All the values were obtained through triplicate tests.

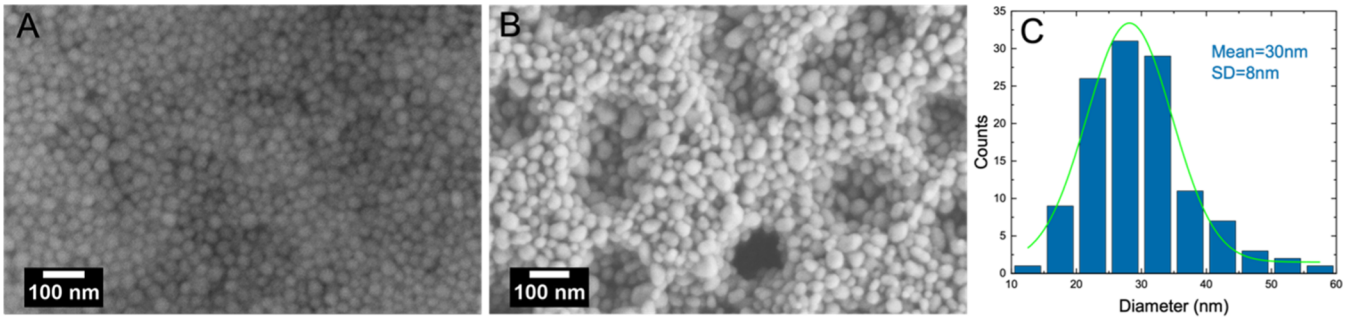


**Figure 5.** (A) SEM image of Ag NPs *via* RC, (B) SEM characterization, and (C) histogram of C−Ag NPs coated on a glass *via* blade-coating (mean size of C−Ag NPs is 30 nm and SD is 8 nm).

significant virus killing rate of up to 99.99% was seen within 30 min of the virus contact with the RC-Ag NPs. Similarly, films made with C−Ag NPs showed a potent virucidal effect with a killing rate of 91.83, 95.25, and 99.97% after an incubation time of 1, 10, and 30 min, respectively. The higher surface roughness observed for the C−Ag NPs layers (Figure S6), compared to that of RC-Ag NPs, is behind the reason for a slightly increased virucidal effect within 10 min. We suspect surface roughness causes a larger area of metal to come in contact with larger number of the viruses, resulting in a higher level of disinfection. Thus, during a 10 min contact period, the disinfection effectivity of the C−Ag NP layer is higher than that of RC-Ag NPs.

The SEM images in Figure 5A,B provide a side-to-side comparison between the two coatings made for this study. An average particle size of 30 ± 8 nm with a distorted spherical shape can be seen for C−Ag NPs. The AFM (Figure S4) study revealed a higher roughness for C−Ag NP layers than those of RC-Ag NPs. Cross-sectional SEM imaging (Figure S7) indicated that the thickness of RC-Ag NPs on glass is 2.26 $\mu$m, which is on the same order as that of C−Ag NPs (1.83 $\mu$m).

*In situ* fabrication of fully effective virucidal mask and textile impregnated with Ag NPs using the *in situ* self-assembly *via* reactive blade coating: RC is a powerful approach to impregnate porous and fibrous substrates with Ag NPs, effectively, as the starting inks are on the molecular level and have a higher penetration ability to sub-nanometer spaces than pre-prepared NPs, limited only by the fluid dynamics at such a scale and interfacial wetting factors between the inks and the substrate material. To empower commercial textiles and face masks against SARS-CoV-2, the reducer ink (Figure 6A) was blade-coated on a single-use face mask, followed by coating silver precursor ink on the top of the reducer ink (Figure 6B).

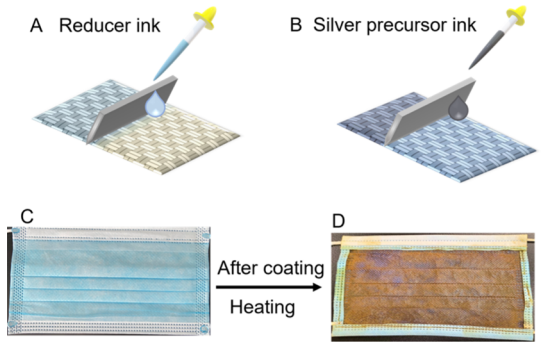


**Figure 6.** *In situ* fabrication process of a Ag NP-impregnated face mask. (A) Coating of the oleylamine-based reducer ink followed by (B) adding the silver precursor ink on top of the previously coated reducer ink. The surface texture of the face mask before (C) and after (D) *in situ* fabrication of Ag NPs *via* RC. The bluish frame shown in D was stitched to the edges of the coated mask, after the heat treatment step, for cosmetic reasons.



https://doi.org/10.1021/acsanm.1c03033
ACS Appl. Nano Mater. 2022, 5, 309−317

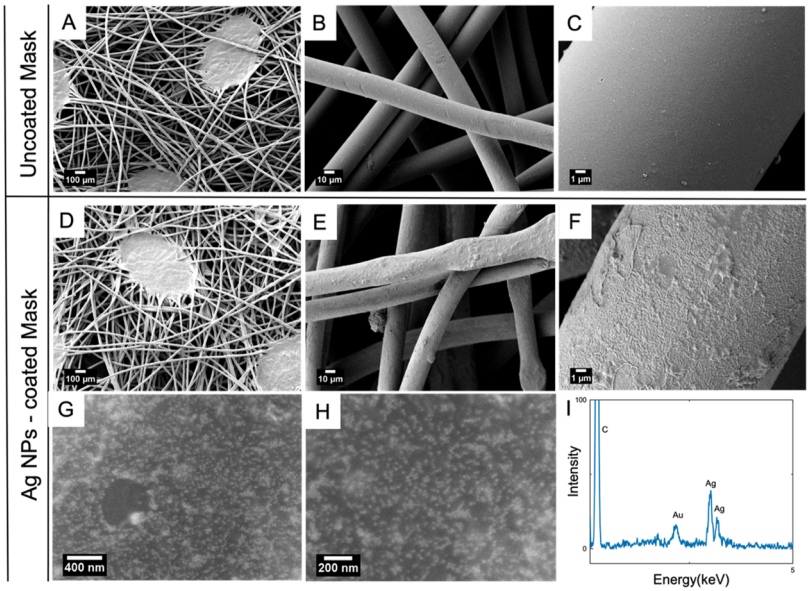


**Figure 7.** SEM images of the (A–C) uncoated mask. (D–F) RC-Ag NP-impregnated mask. (G,H) High-resolution SEM images of the RC-Ag NPs formed on the surface of the mask fibers. (I) EDS spectrum of the Ag NPs formed on the mask, indicating a pure Ag phase without any contamination (Au peak is due to sputtering of 6 nm of Au on the mask prior to SEM imaging).

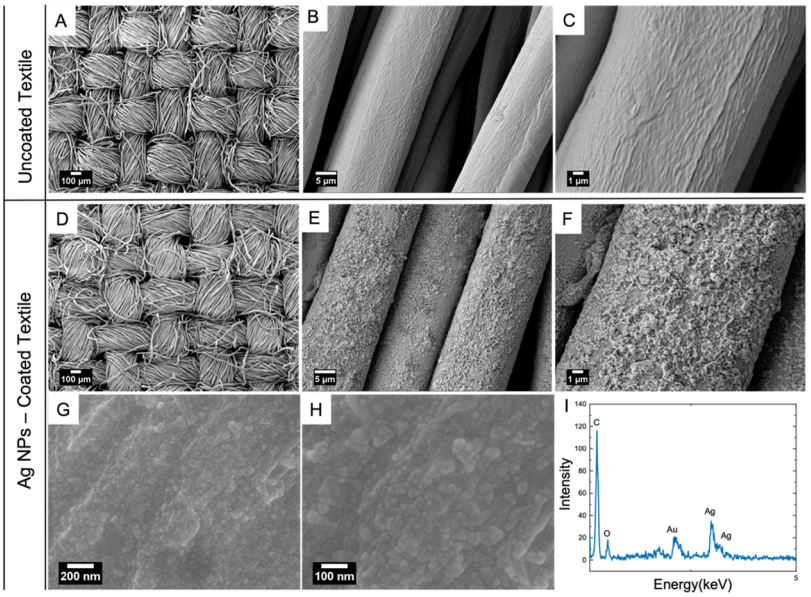


**Figure 8.** SEM images of the cotton fabric without coating (A–C) and RC-Ag NPs impregnated (D–F) at different magnifications. (G,H) High-resolution SEM images of RC-Ag NPs in (D,F) showing the formation of NPs and (I) EDS spectrum of the coated cotton fabric. The Au peak is due to the gold sputtering step needed for better SEM imaging.

Subsequently, a squeezing step using a roller in order to extract the excess reducer and precursor mixed inks was applied. The substrates were then transferred into an oven and heated to 120 °C for 2 h. The single-use face mask before and after reactive impregnation process is shown in Figure 6C,D, respectively. A larger image of the prototype face mask impregnated with Ag NPs *via* RC is reproduced in Figure S8.

In order to enhance the SEM image quality, a thin layer of 5 nm Au was coated on top of the mask substrate. Comparing the SEM images before (Figure 7A–C) and after (Figure 7D–H) coating indicate that the RC process results in the formation of Ag NP coating on the surface of the fibers of the face mask, with an average particle size of ca. (25 ± 4) nm (Figure S9). Content analysis *via* EDS (Figure 7I) confirms that the NP coating is made of pure Ag, whereas the Au peaks is due to the sputtered Au film to facilitate the imaging process.

For the textile substrates made of 100% cotton, the images obtained from the SEM study (Figure 8A–G) reveal the formation of Ag NP coatings. The average size of Ag NPs on textiles is (24 ± 6) nm (Figures 8G and S10). Wetting experiments (Figures S11 and S12) indicate that the cotton textile absorbs both reducer and silver precursor ink very well. Reducer ink is absorbed by the commercial face mask very well while silver precursor ink did not spread completely on the mask due to its hydrophobicity. However, the silver precursor ink wet well on the mask pre-coated with the reducer ink (Figure S7C). The presence of hydroxyl (–OH) groups on the surface of cotton fibers and oxygen sites on polypropylene


https://doi.org/10.1021/acsanm.1c03033
ACS Appl. Nano Mater. 2022, 5, 309–317

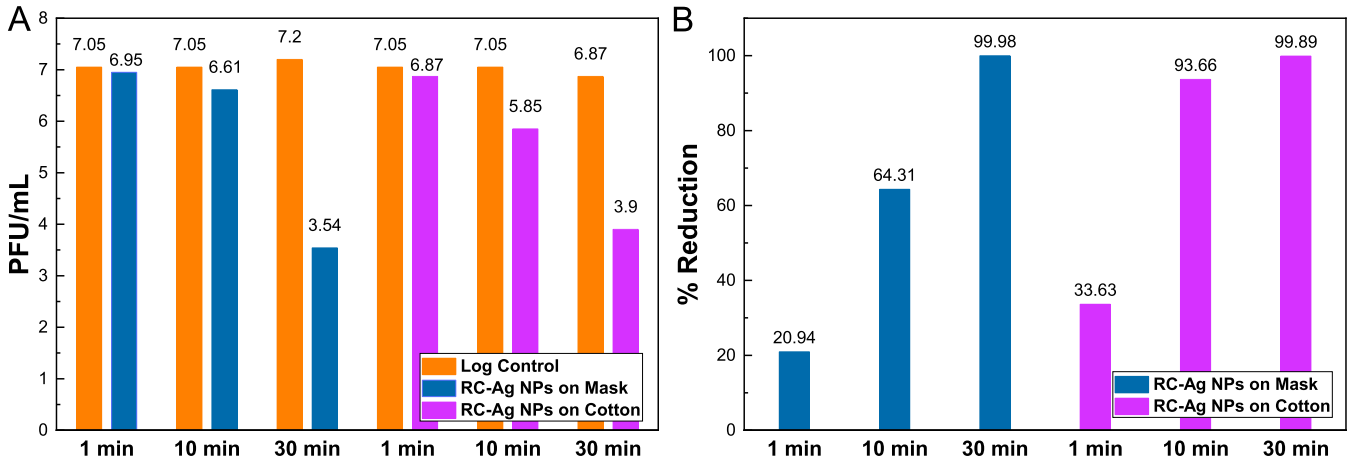


**Figure 9.** (A) Graph illustrating the log geometric mean of HCoV-229E infectivity after contacting the Ag NP-impregnated mask (blue) and textile (purple) for 1, 10, and 30 min, respectively. The orange columns refer to the virus infectivity after contact with the uncoated mask and textile as controls to the related tests. (B) Percent (%) reduction graph represents the efficiency of the Ag NP-impregnated mask and textile to sterilize the HCoV-229E based on the virus infectivity.

contribute to Ag NP adhesion to the textile or polypropylene face mask substrate by providing electrostatic contact with the $Ag^+$ ions. Furthermore, hydrogen bonding between the amine group in oleylamine-capped Ag NPs and −OH (or oxygen) may help the NPs absorb onto the textile fiber.

The antiviral activity test was designed to determine the deactivation of HCoV-229E upon different exposure times to the products, which were the Ag-impregnated mask and cotton fabric samples. The Ag NP-impregnated mask and cotton samples were subsequently incubated for three contact time of 1, 10, and 30 min, respectively, with a 40 $\mu$L of predominantly produced viral load poured on them. After the incubation period, exposed samples to the virus were recovered in 1000 $\mu$L of the media, and the suspensions were then transferred into 10× serial dilution vials and subjected to the plaque-forming assay. For control samples, the virus load was incubated in an uncoated mask and cotton fabric. Our antiviral activity test indicates that the uncoated mask and cotton fabric samples did not show the virucidal effect during the three different incubation times. The log geometric mean of the control medium, Ag NP-impregnated mask, and cotton fabric samples at three different contact times are shown in Figure 9A. In 30 min, both the RC-Ag NPs-impregnated mask and cotton textile exhibit a very high virucidal effect of over 99.9% (Figure 9B). In 1 and 10 min, the Ag NP-impregnated mask reduced the viral activity by 20.94 and 64.31%, respectively, while the Ag NP-impregnated cotton fabric inhibited the viral activity by 33.63 and 93.66%, respectively. In terms of virus inactivation efficacy in 1 and 10 min, Ag NP-impregnated cotton samples outperform their Ag NP-impregnated mask counterparts. Within 30 min, the Ag NP-impregnated face mask *via* RC reached 99.98% virus extinction activity. The higher surface area of the more packed and thinner cotton fibers allows for virus contact with an overall larger area of Ag NPs, which results in a faster disinfection rate for the indicated periods. Antiviral test data for all samples are compiled in Table S1. Regarding cytotoxicity of Ag NPs for the human body, Ag NPs less than 10 nm have been shown to cause cytotoxicity at low concentrations, such as 2 ppm, but larger particles (>10 nm) are safer in terms of cytotoxicity at the same dose.[30] In our work, we believe that an average Ag NP size greater than 25 nm generated by reactive blade coating presents a safer cytotoxicity margin than the previously documented example of 10 nm. However, more detailed experimental results in this regard are needed.

To better understand the wetting behavior between the virus culture media (VCM) and the substrate surface, we measured the contact angle a droplet of VCM without the virus makes with the coated and uncoated (bare) surfaces of the substrate. As expected, the contact angle of VCM for the uncoated mask case was large (ca. 115°, Figure S13A,B) due to the hydrophobicity of the mask material. However, the droplets seem to vanish from the surface by diffusing deeper into the mask within 30 s after contacting the Ag NP coating (Figure S13C−F). This indicates that the hydrophilicity of the mask is affected by the presence of Ag NP coating. On the other hand, the culture media drop spreads very quickly on the surface of uncoated cotton textiles, due to its hydrophilicity, and spreading is somehow inhibited in the presence of Ag NP coating (Figure S1). This behavior can be explained by the cotton threads' closely packed multi-filaments which results in less free space for liquid flow compared to the broader gaps between monofilaments in the mask sample. However, for both cases, virus contact with Ag-NP-coated surfaces of the filaments is rapid, needing only a few dozen seconds, which results in an increased viral inhibition rate as incubation time goes by.

Our results show that RC-Ag NPs on glass, face masks, and cotton textiles are highly effective against HCoV-229E virus. The exact antiviral mechanism of Ag NPs is not fully known yet. Three different mechanisms were proposed to elucidate the antiviral activity: (I) As a soft metal, Ag NPs can penetrate the cell membrane and release $Ag^+$ ions, which shows a strong affinity to react with sulfur residues of glycoproteins of the virus' surface. Furthermore, it interacts with thiol-containing enzyme and effectively prevents virus replication. (II) Its antiviral activity is possibly associated with adhesion (physical interaction) of Ag NPs to the virus surface. This would impede efficient virus docking to the host cell and prevent infecting it. (III) The local generation of reactive oxygen species from the Ag NP surface could be triggered after the docking of Ag NPs on the virus surface, which could damage the envelope and/or membrane of the virus.[2,29,36] Although not discussed here, further studies are needed to understand how the surface


https://doi.org/10.1021/acsanm.1c03033
ACS Appl. Nano Mater. 2022, 5, 309−317

ligand of oleylamine affects the virucidal effect of Ag NPs, and whether it has controlling effects on the release of $Ag^+$ from the Ag NP-coated surfaces.

Our findings could be used in medical personal protective equipment (PPE), hospital bedding, doctors' and patients' attire, furnishings, and packaging, to name a few applications. However, a thorough understanding of the coated film's thickness uniformity on textile fibers, mechanical properties (such as tensile strength, stretching, and bending), stability when exposed to physiological fluids (such as breath and saliva), $Ag^+$ ions' release rate from the film over time, and cytotoxicity must first be established.

## CONCLUSIONS

To mitigate the widespread of SARS-CoV-2, we presented a R2R compatible technique, namely, reactive blade coating, and showed its success in fabricating antiviral Ag NP coating with a high viricidal effectivity against a surrogate virus such as HCov-229E on rigid substrates and flexible ones in the form of face masks and cotton textiles. A disinfection rate of 99.98% within 30 min was reached for the face mask and 99.99% for the glass substrate. We believe that the safe and effective antiviral function of our *in situ* RC process can be integrated into the broader spectrum of PPE at an industrial scale. SEM and EDS studies revealed that RC-Ag NPs on various substrates are made up of pure silver.

## MATERIALS AND METHODS

**Materials.** Organic solvents, including TOL and DMSO, were used for preparing the inks for the RC synthesis of Ag NPs. Silver nitrate $AgNO_3$ was used as the silver precursor and oleylamine as the reducing agent. Solvents including acetone and ethanol were used in cleaning the glass slides. All of the above-mentioned chemicals were obtained from Sigma-Aldrich. Carbon steel sterile surgical blades, obtained from Kai Industries Co. (Japan), were utilized for the blade coating process.

HCoV-229E virus (ATCC #VR-740) and L132 cell line (ATCC CCL-5) were provided from the Bioanalytical and Molecular Interaction (BioAMI) Laboratory at the department of chemistry and biomolecular sciences at the uOttawa. The culture medium and neutral red Cat# N6264-50ML for staining viable cells were obtained from Sigma-Aldrich. Silver NP conductive ink was obtained from BotFactory (USA).

**Sample Preparation.** The glass slides were first rinsed with deionized water followed by a 10 min ultrasonic bath in acetone, ethanol, and IPA. The samples were dried with airflow after each bath.

**Thin Film Characterization.** Various characterization techniques were used to characterize both the RC-Ag NP thin films and the commercial Ag NP ink-coated films on glass slides, face masks, and cotton substrates. SEM, using a Zeiss Gemini 500, was performed to analyze the morphology and size distribution of the NPs. A UV−vis spectrometer (Carry 7000) was employed to identify the plasmonic behavior of Ag NP coatings and analyze their optical properties. Additionally, the crystallographic phase of the blade-coated thin film was investigated using an X-ray diffractometer (Rigaku Ultima IV diffractometer). To measure the surface roughness of the substrates, surface atomic force microscopy (AFM) was carried out.

**Virus Assay.** The HCoV-229E (ATCC #VR-740) was propagated in the L-132 cell line (ATCC #CCL-5) for the experiments. The L-132 cell line was developed from human embryonic lung tissue and growth in α-EM (GIBCO-BRL Cat # 41600-016) in the presence of L-glutamine and 10% FBS. The virus was propagated by adding 200 μL of the virus with titration of one plaque per cell on the L-132 cell monolayer in a T-75 cell culture flask and incubated in a cell culture incubator at 35 °C and 5% $CO_2$. The solution was replaced by α-MEM with 2% FBS and incubated at 35 °C and 5% $CO_2$ before the cytopathic effect appeared. The propagated virus was harvested after three freeze−thaw cycles, followed by a centrifuge with 1000*g* for 10 min. The pool was aliquoted and stored at 4 °C. An aliquot of the harvested virus pool was titrated by plaque-forming assay.

**Testing.** The test method here followed ASTM E1153-03 Standard Test Method for Efficacy of Sanitizers Recommended for Inanimate Non-Food Contact Surfaces and CAN/CGSB-2.161-97 for Assessment of Efficacy of Antimicrobial Agents for Use on Environmental Surfaces and Medical Devices. The HCoV-229E stock was prepared in a soil load with a final concentration of 5% FBS. The triplicated tests were planned to examine the NPs disinfection efficiency.

Results were also calculated accordingly, following ASTM E1153—03, Standard Test Method for Efficacy of Sanitizers Recommended for Inanimate Non-Food Contact Surfaces CAN/CGSB-2.161-97, Assessment of Efficacy of Antimicrobial Agents for Use on Environmental Surfaces and Medical Devices. In this case, two 10× dilution of HCoV-229E stock was prepared in a soil load with a final concentration of 5% FBS. A 40 μL volume of the resulting mixture was poured on the NP-coated thin film/mask/cotton textile (one by one inch) and incubated for three different contact times of 1, 10, and 30 min. After each contact time, virus-exposed slides were recovered in 1000 μL of the media. The suspensions were then transferred into 10× serial dilution vials and subjected to the plaque forming assay. All the control samples used in the experiments were also prepared by incubating the same virus pool on the glass slide/mask/cotton textile but with no NPs.

The plaque-forming assays were conducted by replacing 100 μL of appropriated dilution with the media of the L-132 cells monolayer cultured in six-well plates. The plates were incubated at 35 °C in a 5% $CO_2$ atmosphere for 60 min. The solution in each well was replaced with 2 mL of medium supplemented by 2% FBS and 0.5% low melting agarose and then incubated at 35 °C in a 5% $CO_2$ incubator. The second layer of agarose media, including 0.03% of neutral red (Sigma-Aldrich, Cat# N6264-50ML), was added on the 4th day. The neutral red stains live cells, which improves the monitoring of the plaque formation. Upon developing the plaques, the cells were fixed by adding 10% buffered formalin. After three hours, the overlays were removed, and cells were washed and stained with 0.5% crystal violet. After rinsing the plates, the plaques appeared with a distinct form specific to HCoV-229E, and they were counted. Geometric mean, percent reduction, and log reduction were calculated according to ASTM E1153—03, ASTM (Standard Test Method for Efficacy of Sanitizers Recommended for Inanimate Non-Food Contact Surfaces). The coated samples were maintained under vacuum for 8 days before biological testing.

## ASSOCIATED CONTENT

### Supporting Information

The Supporting Information is available free of charge at https://pubs.acs.org/doi/10.1021/acsanm.1c03033.

Images of RC-Ag NPs and C−Ag NPs on glass; EDS of spectra of RC-Ag NPs on glass; SEM images and XRD spectra of RC-Ag NP films synthesized by various solvent systems; images of cell growth and confluence during plaque formation compared to control cells at different time points; antiviral test data for all samples; AFM and cross-sectional SEM characterizations of RC-Ag NP and C−Ag NP films; image of the RC-Ag NP-coated full face mask; histograms of Ag NPs formed on the face mask and cotton via RC; and contact angle measurements of inks on the face mask and cotton (PDF)



https://doi.org/10.1021/acsanm.1c03033
ACS Appl. Nano Mater. 2022, 5, 309−317

## AUTHOR INFORMATION


### Corresponding Author

**Ghassan E. Jabbour** − *School of Electrical Engineering and Computer Science, University of Ottawa, Ottawa, Ontario K1N 6N5, Canada*; Email: gja@uottawa.ca

### Authors

**Mutalifu Abulikemu** − *School of Electrical Engineering and Computer Science, University of Ottawa, Ottawa, Ontario K1N 6N5, Canada*; orcid.org/0000-0002-8848-6804

**Bita E. A. Tabrizi** − *School of Electrical Engineering and Computer Science, University of Ottawa, Ottawa, Ontario K1N 6N5, Canada*

**Shahrokh M. Ghobadloo** − *Flow Cytometry and Robotic Facility, Faculty of Science, University of Ottawa, Ottawa, Ontario K1N 6N5, Canada*

**Hamed M. Mofarah** − *School of Electrical Engineering and Computer Science, University of Ottawa, Ottawa, Ontario K1N 6N5, Canada*

Complete contact information is available at: https://pubs.acs.org/10.1021/acsanm.1c03033


### Notes

The authors declare no competing financial interest.

## ACKNOWLEDGMENTS

The figure in TOC was created in part by https://biorender.com/. The authors acknowledge the support of Canadian government through the Canada Research Chair (Tier 1) (award # 950-231466) and NSERC Discovery Grant (award # RGPIN- 2020-06970).

## REFERENCES


(1) Gurunathan, S.; Qasim, M.; Choi, Y.; Do, J. T.; Park, C.; Hong, K.; Kim, J.-H.; Song, H. Antiviral Potential of Nanoparticles—Can Nanoparticles Fight against Coronaviruses? *Nanomaterials* **2020**, *10*, 1645.

(2) Weiss, C.; Carriere, M.; Fusco, L.; Capua, I.; Regla-Nava, J. A.; Pasquali, M.; Scott, J. A.; Vitale, F.; Unal, M. A.; Mattevi, C.; Bedognetti, D.; Merkoçi, A.; Tasciotti, E.; Yilmazer, A.; Gogotsi, Y.; Stellacci, F.; Delogu, L. G. Toward Nanotechnology-Enabled Approaches against the COVID-19 Pandemic. *ACS Nano* **2020**, *14*, 6383−6406.

(3) Bucknall, R. A.; King, L. M.; Kapikian, A. Z.; Chanock, R. M. Studies with Human Coronaviruses. II. Some Properties of Strains 229E and OC43. *Proc. Soc. Exp. Biol. Med.* **1972**, *139*, 722−727.

(4) van Doremalen, N.; Bushmaker, T.; Morris, D. H.; Holbrook, M. G.; Gamble, A.; Williamson, B. N.; Tamin, A.; Harcourt, J. L.; Thornburg, N. J.; Gerber, S. I.; Lloyd-Smith, J. O.; de Wit, E.; Munster, V. J. Aerosol and Surface Stability of SARS-CoV-2 as Compared with SARS-CoV-1. *N. Engl. J. Med.* **2020**, *382*, 1564−1567.

(5) Talebian, S.; Wallace, G. G.; Schroeder, A.; Stellacci, F.; Conde, J. Nanotechnology-based Disinfectants and Sensors for SARS-CoV-2. *Nat. Nanotechnol.* **2020**, *15*, 618−621.

(6) Imani, S. M.; Ladouceur, L.; Marshall, T.; Maclachlan, R.; Soleymani, L.; Didar, T. F. Antimicrobial Nanomaterials and Coatings: Current Mechanisms and Future Perspectives to Control the Spread of Viruses Including SARS-CoV-2. *ACS Nano* **2020**, *14*, 12341−12369.

(7) Bobrin, V. A.; Chen, S.-P.; Grandes Reyes, C. F.; Sun, B.; Ng, C. K.; Kim, Y.; Purcell, D.; Jia, Z.; Gu, W.; Armstrong, J. W.; McAuley, J.; Monteiro, M. J. Water-Borne Nanocoating for Rapid Inactivation of SARS-CoV-2 and Other Viruses. *ACS Nano* **2021**, *15*, 14915−14927.

(8) Kampf, G.; Todt, D.; Pfaender, S.; Steinmann, E. Persistence of Coronaviruses on Inanimate Surfaces and Their Inactivation with Biocidal Agents. *J. Hosp. Infect.* **2020**, *104*, 246−251.

(9) Hallsworth, L. https://rilleatechnologies.com/epa-approved-disinfectants-for-coronavirus/ (accessed Nov 7, 2021).

(10) Huang, H.; Fan, C.; Li, M.; Nie, H.-L.; Wang, F.-B.; Wang, H.; Wang, R.; Xia, J.; Zheng, X.; Zuo, X.; Huang, J. COVID-19: A Call for Physical Scientists and Engineers. *ACS Nano* **2020**, *14*, 3747−3754.

(11) Medhi, R.; Srinoi, P.; Ngo, N.; Tran, H.-V.; Lee, T. R. Nanoparticle-Based Strategies to Combat COVID-19. *ACS Appl. Nano Mater.* **2020**, *3*, 8557−8580.

(12) Serrano-Aroca, Á.; Takayama, K.; Tuñón-Molina, A.; Seyran, M.; Hassan, S. S.; Pal Choudhury, P.; Uversky, V. N.; Lundstrom, K.; Adadi, P.; Palù, G.; Aljabali, A. A. A.; Chauhan, G.; Kandimalla, R.; Tambuwala, M. M.; Lal, A.; Abd El-Aziz, T. M.; Sherchan, S.; Barh, D.; Redwan, E. M.; Bazan, N. G.; Mishra, Y. K.; Uhal, B. D.; Brufsky, A. Carbon-based Nanomaterials: Promising Antiviral Agents to Combat COVID-19 in the Microbial-Resistant era. *ACS Nano* **2021**, *15*, 8069−8086.

(13) Balasubramaniam, B.; Prateek; Ranjan, S.; Saraf, M.; Kar, P.; Singh, S. P.; Thakur, V. K.; Singh, A.; Gupta, R. K. Antibacterial and Antiviral Functional Materials: Chemistry and Biological Activity toward Tackling COVID-19-like Pandemics. *ACS Pharmacol. Transl. Sci.* **2021**, *4*, 8−54.

(14) Khurana, A.; Allawadhi, P.; Khurana, I.; Allwadhi, S.; Weiskirchen, R.; Banothu, A. K.; Chhabra, D.; Joshi, K.; Bharani, K. K. Role of nanotechnology behind the success of mRNA vaccines for COVID-19. *Nano Today* **2021**, *38*, 101142.

(15) Vazquez-Munoz, R.; Lopez-Ribot, J. L. Nanotechnology as an Alternative to Reduce the Spread of COVID-19. *Challenges* **2020**, *11*, 15.

(16) Karim, N.; Afroj, S.; Lloyd, K.; Oaten, L. C.; Andreeva, D. V.; Carr, C.; Farmery, A. D.; KimNovoselov, I. D. K. S. Sustainable Personal Protective Clothing for Healthcare Applications: A Review. *ACS nano* **2020**, *14*, 12313−12340.

(17) Nakamura, S.; Sato, M.; Sato, Y.; Ando, N.; Takayama, T.; Fujita, M.; Ishihara, M. Synthesis and Application of Silver Nanoparticles (Ag NPs) for the Prevention of Infection in Healthcare Workers. *Int. J. Mol. Sci.* **2019**, *20*, 3620.

(18) Allawadhi, P.; Singh, V.; Khurana, A.; Khurana, I.; Allwadhi, S.; Kumar, P.; Banothu, A. K.; Thalugula, S.; Barani, P. J.; Naik, R. R.; Bharani, K. K. Silver nanoparticle based multifunctional approach for combating COVID-19. *Sensors Int.* **2021**, *2*, 100101.

(19) Das Jana, I.; Kumbhakar, P.; Banerjee, S.; Gowda, C. C.; Kedia, N.; Kuila, S. K.; Banerjee, S.; Das, N. C.; Das, A. K.; Manna, I.; Tiwary, C. S. Copper Nanoparticle−Graphene Composite-Based Transparent Surface Coating with Antiviral Activity against Influenza Virus. *ACS Appl. Nano Mater.* **2021**, *4*, 352−362.

(20) Qi, M.; Li, W.; Zheng, X.; Li, X.; Sun, Y.; Wang, Y.; Li, C.; Wang, L. Cerium and its oxidant-based nanomaterials for antibacterial applications: a state-of-the-art review. *Front. Mater. Sci.* **2020**, *7*, 213.

(21) Cagno, V.; Andreozzi, P.; D'Alicarnasso, M.; Jacob Silva, P.; Mueller, M.; Galloux, M.; Le Goffic, R.; Jones, S. T.; Vallino, M.; Hodek, J.; Weber, J.; Sen, S.; Janeček, E.-R.; Bekdemir, A.; Sanavio, B.; Martinelli, C.; Donalisio, M.; Rameix Welti, M.-A.; Eleouet, J.-F.; Han, Y.; Kaiser, L.; Vukovic, L.; Tapparel, C.; Král, P.; Krol, S.; Lembo, D.; Stellacci, F. Broad-spectrum non-toxic antiviral nanoparticles with a virucidal inhibition mechanism. *Nat. Mater.* **2018**, *17*, 195−203.

(22) Ghaffari, H.; Tavakoli, A.; Moradi, A.; Tabarraei, A.; Bokharaei-Salim, F.; Zahmatkeshan, M.; Farahmand, M.; Javanmard, D.; Kiani, S. J.; Esghaei, M.; Pirhajati-Mahabadi, V.; Monavari, S. H.; Ataei-Pirkooh, A. Inhibition of H1N1 Influenza Virus Infection by Zinc Oxide Nanoparticles: Another Emerging Application of Nanomedicine. *J. Biomed. Sci.* **2019**, *26*, 70.

(23) Ren, G.; Hu, D.; Cheng, E. W. C.; Vargas-Reus, M. A.; Reip, P.; Allaker, R. P. Characterisation of Copper Oxide Nanoparticles for Antimicrobial Applications. *Int. J. Antimicrob. Agents* **2009**, *33*, 587−590.

(24) Varaprasad, K.; Raghavendra, G. M.; Jayaramudu, T.; Seo, J. Nano Zinc Oxide−Sodium Alginate Antibacterial Cellulose Fibres. *Carbohydr. Polym.* **2016**, *135*, 349−355.
(25) Adhikari, A.; Pal, U.; Bayan, S.; Mondal, S.; Ghosh, R.; Darbar, S.; Saha-Dasgupta, T.; Ray, S. K.; Pal, S. K. Nanoceutical Fabric Prevents COVID-19 Spread through Expelled Respiratory Droplets: A Combined Computational, Spectroscopic, and Antimicrobial Study. *ACS Appl. Bio Mater.* **2021**, *4*, 5471−5484.
(26) Borkow, G.; Zhou, S. S.; Page, T.; Gabbay, J. A Novel Anti-Influenza Copper Oxide Containing Respiratory Face Mask. *PLoS One* **2010**, *5*, No. e11295.
(27) Galdiero, S.; Falanga, A.; Vitiello, M.; Cantisani, M.; Marra, V.; Galdiero, M. Silver Nanoparticles as Potential Antiviral Agents. *Molecules* **2011**, *16*, 8894−8918.
(28) Balagna, C.; Perero, S.; Percivalle, E.; Nepita, E. V.; Ferraris, M. Virucidal Effect Against Coronavirus SARS-CoV-2 of a Silver Nanocluster/Silica Composite Sputtered Coating. *Open Ceramics* **2020**, *1*, 100006.
(29) Tremiliosi, G. C.; Simoes, L. G. P.; Minozzi, D. T.; Santos, R. I.; Vilela, D. C. B.; Durigon, E. L.; Machado, R. R. G.; Medina, D. S.; Ribeiro, L. K.; Rosa, I. L. V.; Assis, M.; Andrés, J.; Longo, E.; Freitas-Junior, L. H. Ag nanoparticles-based antimicrobial polycotton fabrics to prevent the transmission and spread of SARS-CoV-2. **2020**, (Preprint) BioRxiv:152520, submitted: June 2020.
(30) Jeremiah, S. S.; Miyakawa, K.; Morita, T.; Yamaoka, Y.; Ryo, A. Potent antiviral effect of silver nanoparticles on SARS-CoV-2. *Biochem. Biophys. Res. Commun.* **2020**, *533*, 195−200.
(31) Ikner, L. A.; Torrey, J. R.; Gundy, P. M.; Gerba, C. P. A Continuously Active Antimicrobial Coating Effective against Human Coronavirus 229E. **2020**, (Preprint) medRxiv:20097329, submitted: May 2020.
(32) Huang, L.; XuWang, S. Z.; Xue, K.; Su, J.; Song, Y.; Chen, S.; Zhu, C.; Tang, B. Z.; Ye, R. Self-Reporting and Photothermally Enhanced Rapid Bacterial Killing on a Laser-Induced Graphene Mask. *ACS Nano* **2020**, *14*, 12045−12053.
(33) Kumaran, S.; Oh, E.; Han, S.; Choi, H.-J. Photopolymerizable, Universal Antimicrobial Coating to Produce High-Performing, Multifunctional Face Masks. *Nano Lett.* **2021**, *21*, 5422−5429.
(34) Tania, I. S.; Ali, M.; Bhuiyan, R. H. Experimental Study on Dyeing Performance and Antibacterial Activity of Silver Nanoparticle-Immobilized Cotton Woven Fabric. *Autex Res. J.* **2021**, *21*, 45−51.
(35) Zhu, J.; Li, B.; Xu, M.; Liu, R.; Xia, T.; Zhang, Z.; Xu, Y.; Liu, S. Graphene Oxide Promotes Cancer Metastasis through Associating with Plasma Membrane to Promote TGF-$\beta$ Signaling-Dependent Epithelial−Mesenchymal Transition. *ACS Nano* **2020**, *14*, 818−827.
(36) Salleh, A.; Naomi, R.; Utami, N. D.; Mohammad, A. W.; Mahmoudi, E.; Mustafa, N.; Fauzi, M. B. The Potential of Silver Nanoparticles for Antiviral and Antibacterial Applications: A Mechanism of Action. *Nanomaterials* **2020**, *10*, 1566.




https://doi.org/10.1021/acsanm.1c03033
*ACS Appl. Nano Mater.* 2022, 5, 309−317